Optics Letters

Perfect space–time vortices

Sergey A. Ponomarenko[1,2,*] and Davud Hebri[2]

[1]Department of Electrical and Computer Engineering, Dalhousie University, Halifax, Nova Scotia, B3J 2X4, Canada
[2]Department of Physics and Atmospheric Science, Dalhousie University, Halifax, Nova Scotia, B3H 4R2, Canada
*serpo@dal.ca

Received 8 May 2024; revised 26 June 2024; accepted 10 July 2024; posted 11 July 2024; published 23 July 2024

We introduce the concept of perfect space–time vortices (PSTVs) that can exist in media with anomalous dispersion. If the topological charge of a PSTV is not too large, the spatiotemporal intensity distribution of the vortex field does not depend on the magnitude of the topological charge. We show theoretically how a PSTV can be realized in the optical context through spatiotemporal focusing of a Bessel–Gaussian space–time optical vortex source that is placed in the focal plane of a space–time lens composed of an ordinary lens and a time lens with matched spatial and temporal focal lengths.

https://doi.org/10.1364/OL.529611

Optical vortices (OVs) are structured light fields with helicoidal wavefronts surrounding the lines of zero intensity [1,2]. The correlation functions of random optical fields can also be endowed with vortices [3,4]. Since the seminal discovery of a connection between an optical vortex and the orbital angular momentum (OAM) of light [5], many intriguing fundamental aspects of OVs and OAM have been unveiled and numerous applications emerged of OVs to optical communications [6,7], optical trapping and tweezing [8,9], imaging [10], and even optical computing [11].

A garden variety OV exhibits a characteristic intensity null on its axis which is surrounded by a bright ring with the radius scaling with the magnitude of its OAM [6,12]. This state of affairs is troublesome for some applications. For instance, optical communication protocols greatly benefit from multiplexing as many spatially overlapping OAM states as possible [13]. By the same token, it is often desirable that the size of a trapping vortex beam be independent of its OAM content [14]. The so-called perfect vortex beams were introduced [15] and actively explored [16,17] to accommodate such situations. The intensity profile of a realistic perfect vortex forms a thin ring of a radius nearly independent of the topological charge of the vortex [18].

In addition to OVs carrying longitudinal OAM, which have been extensively studied to date, spatiotemporal optical vortices (STOVs), supported by dispersive optical media and endowed with transverse OAM, have recently piqued researchers' curiosity [19]. The spatiotemporal vortices have been theoretically suggested [20] and experimentally realized [21,22], and several classes of STOVs, including dispersionless [23] and dispersive [24] Bessel and Laguerre–Gaussian ones [25], were examined in detail. As STOVs rely on tight coupling between spatial and temporal degrees of freedom of optical fields, they present fundamental interest. In this connection, a question arises: Is it possible to generate a perfect space–time optical vortex in a dispersive medium?

In this Letter, we introduce the concept of perfect space–time vortices (PSTVs). The spatiotemporal field distribution of any PSTV is independent of its OAM content. We show that in the optical context, a PSTV can be generated upon focusing a Bessel–Gauss space–time vortex source with a sequence of an ordinary lens and a time lens with matched spatial and temporal focal lengths. We also compare and contrast the energy density flux of Bessel–Gauss and perfect space–time vortex fields. We anticipate the discovered PSTVs to find applications to dynamic trapping and tweezing neutral particles along controllable space–time trajectories as well as to optical communications with pulsed light fields.

The evolution of the electric field $\mathbf{E}$ in a linear isotropic, weakly dispersive medium is governed, in the space–frequency domain, by the Helmholtz wave equation of the form

$$\nabla'^2\mathbf{E} + \beta^2(\omega')\mathbf{E} = 0. \tag{1}$$

Here $\beta(\omega')$ is a propagation constant of a plane wave of frequency ω' in the medium. Hereafter, all primed variables are dimensional. Assuming a linearly polarized electric field, we can write the field in terms of its slowly varying space–time envelope Ψ as

$$\mathbf{E}(x',t',z') = \mathbf{e}_y\Psi(x',t',z')e^{i(\beta_0 z' - \omega_0' t')}, \tag{2}$$

where ω_0' is a carrier frequency, $\beta_0 = \beta(\omega_0')$, and $\mathbf{e}_y$ is a unit vector in the y-direction. We can then express Ψ in terms of its angular spectrum as follows:

$$\Psi(x',t',z') = \int dk_x' \int d\Omega'\, \mathcal{A}(k_x',\Omega')e^{iq_z z'}e^{ik_x' x'}e^{-i\Omega' t'}. \tag{3}$$

Here $q_z = k_z' - \beta_0$, $\Omega' = \omega' - \omega_0'$ and $\mathcal{A}(k_x',\Omega') = \widetilde{\Psi}(x',t',0)$, tilde denoting a Fourier transform, is a (complex) spectral amplitude of the field. Further, the wave vector of each plane wave of the angular spectrum satisfies the dispersion relation as

$$k_z'^2 + k_x'^2 = \beta^2(\Omega'), \tag{4}$$

where we assumed that the field is collimated in the y-direction (light sheet), which is typically required to ensure tight space-time coupling among the (k_x',Ω') pairs of the angular spectrum [26].

Next, weak dispersion implies negligible absorption. We can then expand the propagation constant as

$$\beta(\Omega') \simeq \beta_0 + \beta_1\Omega' + \beta_2\Omega'^2/2. \tag{5}$$

Here β_1 and β_2 describe the (inverse) group velocity at frequency ω_0' and group velocity dispersion, respectively, while the paraxiality of the envelope, together with Eq. (5), allows us to transform Eq. (4) to

$$q_z \simeq \beta_1\Omega' + \beta_2\Omega'^2/2 - k_x'^2/(2\beta_0). \tag{6}$$

On substituting from Eqs. (5) and (6) into Eq. (3), we can cast the angular spectrum representation for Ψ into the form

$$\Psi(x',t',z') = \int dk_x' \int d\Omega'\, \mathcal{A}(k_x',\Omega') e^{i(k_x'x' - \Omega'\tau')} \times e^{iz'(\beta_2\Omega'^2 - k_x'^2/\beta_0)/2}, \tag{7}$$

where we introduced a retarded time by the expression $\tau' = t' - \beta_1 z'$.

At this stage, it is convenient to transform to dimensionless variables by scaling the coordinates (x',τ') and (k_x',Ω') in physical and reciprocal spaces, respectively, to characteristic scales σ_x and σ_t as $x = x'/\sigma_x$ and $\tau = \tau'/\sigma_t$ as well as $K = k_x'\sigma_x$ and $\Omega = \Omega'\sigma_t$. Further, introducing characteristic diffraction and dispersion lengths by $L_x = 2\beta_0\sigma_x^2$ and $L_t = 2\sigma_t^2/|\beta_2|$, we can scale the longitudinal coordinate as $z = z'/L_d$ where $L_d = \sqrt{L_xL_t}$. The field envelope in dimensionless coordinates then reads

$$\Psi(x,t,z) = \int dK \int d\Omega\, \mathcal{A}(K,\Omega) e^{i(Kx - \Omega\tau)} e^{iz(as\Omega^2 - K^2/a)}. \tag{8}$$

Here $s = \mathrm{sgn}(\beta_2)$ and $a = \sqrt{L_x/L_t}$ is a stretching factor quantifying the relative strength of diffraction and dispersion. We can infer at once from Eq. (8) that the physics of any envelope evolution is completely determined by its spectral amplitude, the type of medium dispersion—normal versus anomalous—and the stretching factor.

Further, the angular spectrum representation [Eq. (8)] can be shown to be equivalent to a paraxial wave equation for the field envelope in the form

$$ia\partial_z\Psi + \partial_{xx}^2\Psi - sa^2\partial_{\tau\tau}^2\Psi = 0. \tag{9}$$

Following Ref. [27] and introducing the amplitude and phase of Ψ, such that $\Psi = |\Psi|e^{i\Phi}$, we can readily derive a continuity equation for the energy density $|\Psi|^2$ as

$$\partial_z|\Psi|^2 + \nabla\cdot\mathbf{J} = 0, \tag{10}$$

where the energy density flux reads

$$\mathbf{J} = (2a^{-1}\mathbf{e}_x\partial_x\Phi - 2as\mathbf{e}_\tau\partial_\tau\Phi)|\Psi|^2. \tag{11}$$

The circulation of $\mathbf{J}$ around a vortex core is a fundamental signature of any space–time optical vortex.

Let us now focus on the anomalous dispersion case, $s = -1$. It will prove convenient to transform to stretched polar coordinates that we define as

$$K = a^{1/2}\kappa\cos\theta, \qquad \Omega = a^{-1/2}\kappa\sin\theta, \tag{12a}$$

$$x = a^{-1/2}r\cos\phi, \qquad \tau = a^{1/2}r\sin\phi. \tag{12b}$$

It follows at once from Eq. (12) that

$$\kappa = \sqrt{K^2/a + a\Omega^2}, \qquad \theta = \arctan[a\Omega/K], \tag{13a}$$

$$r = \sqrt{ax^2 + \tau^2/a}, \qquad \phi = \arctan[\tau/(ax)]. \tag{13b}$$

Next, consider the angular spectrum constrained to an ellipse in the k-space such that

$$\mathcal{A}_\mathrm{B}(\kappa,\theta) \propto \delta(\kappa - 1)e^{-il\theta}. \tag{14}$$

Henceforth, we drop any immaterial normalization constant. It follows at once from Eqs. (8) and (14), upon some algebra spelled out in Supplement 1, that

$$\Psi_\mathrm{B}(r,\phi,z) \propto J_l(r)e^{il\phi}, \tag{15}$$

which describes an ideal propagation-invariant space–time Bessel vortex previously studied in [24]. Unfortunately, just like its infinite-power spatial counterpart [28,29], such a field carries infinite energy and hence cannot be realized in the laboratory. A finite-energy realization of such a space–time vortex can be obtained by utilizing the spectral amplitude:

$$\mathcal{A}_\mathrm{BG}(\kappa,\theta) \propto I_l(2p\kappa)e^{-\kappa^2}e^{-il\theta}, \tag{16}$$

where p is a real parameter and $I_l(x)$ is a modified Bessel function of the first kind and order l. We sketch $|\mathcal{A}_\mathrm{BG}(\kappa,\theta)|$ as a function of κ in Fig. 1. We can infer from the figure that for $p \gg 1$, the angular spectrum is virtually independent of l and sharply peaks around $\kappa_\mathrm{max} \simeq p$. Notice, though, that the angular spectrum peak slightly shifts away from κ_max for sufficiently large l, and this trend is mitigated by employing greater p as is seen in the bottom panel of the figure. We also exhibit an approximate expression for the angular spectrum obtained with the aid of an asymptotic expression for the modified Bessel function for large arguments—see Supplement 1 for details–with a solid blue line in the top and middle panels of the figure.

On substituting from Eq. (16) into Eq. (8), we obtain, after straightforward manipulations detailed in Supplement 1, for the

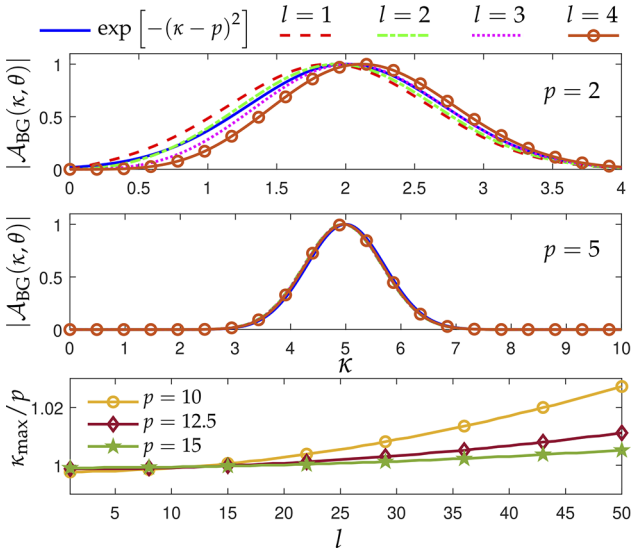

Fig. 1. Top and middle rows: absolute value of the spectral amplitude of an STBG vortex of variables l and p. Bottom row: the position of the peak of the angular spectrum amplitude versus l for variable p. Solid blue line: asymptotic expression for the absolute value of the spectral amplitude.

field envelope the following expression:

$$\Psi_{\mathrm{BG}}(r,\phi,z) \propto \frac{e^{il\phi}}{(1+iz)} \exp\left(\frac{p^2 - r^2/4}{1+iz}\right) J_l\left(\frac{pr}{1+iz}\right). \tag{17}$$

Equation (17) defines a space–time Bessel–Gauss (STBG) beam carrying an elliptic vortex of topological charge l.

We display the evolution of intensity, phase, and energy density flux of an STBG vortex as functions of z in Fig. 2. The most remarkable feature manifest from Fig. 2 is vanishing of the vortex on the propagation of the STBG beam. Indeed, we can observe by comparing the panels in the top and third from the top rows of the figure that the energy flow, which circulates around the vortex core at the source, gradually changes its direction, transforming into a purely radial flux at $z = 0.4$. Hence, we can conclude that, in general, the STBG field loses its vortex structure at a certain distance on propagation in a linear dispersive medium.

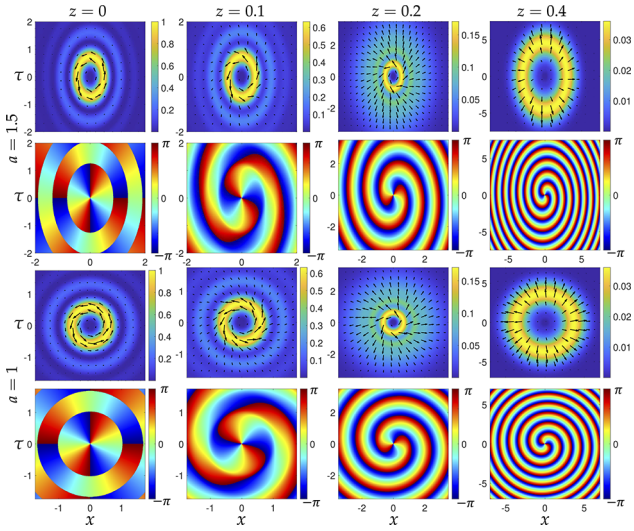

Fig. 2. Evolution of the intensity, phase, and energy density flow (depicted by arrows over the intensity profiles) of STBG vortices with $l = 2$, $p = 5$, and variable a.

We now show how a perfect space–time vortex can be generated from an STBG beam if we rely on focusing instead of diffraction. To this end, we introduce the concept of a space–time lens. We assume the source field is transmitted through a time lens imposing a linear temporal chirp C onto the field, followed by an ordinary lens of focal length f. In practice, the time lens is typically realized [30] by having an optical probe and microwave control fields co-propagate over a short distance inside a waveguide. The microwave field then imparts a quadratic temporal phase to the optical one via a linear [31] or quadratic [32] electro-optical effect.

We now treat space–time focusing quantitatively inspired by the standard textbook approach to spatial lensing [33]. We can infer from Eq. (8) that the complex amplitudes of Ψ in any transverse plane $z = const \geq 0$ and at the source are related via a (stretched) space–time Fresnel transform as

$$\Psi(x,\tau,z) = \left(\frac{1}{4\pi i z}\right) \int d\xi \int d\zeta\, \Psi(\xi,\zeta,0) \times \exp\left[\frac{i}{4z}\left(a(x-\xi)^2 + (\tau-\zeta)^2/a\right)\right]. \tag{18}$$

Let us assume that the source is located right behind a thin ordinary lens of focal length f and the time lens so that

$$\Psi_l^+(x,\tau,0) = \Psi_l^-(x,\tau,0) e^{-iL_x x^2/(4f)} e^{-iC\tau^2}. \tag{19}$$

Here the field right in front of (behind) the space–time lens is denoted with the superscript + (−); we employ the subscript "l" to stress that the field envelope is evaluated right in the transverse plane of the lens. Assuming the source plane coincides with the plane of the lens and substituting from Eq. (19) into Eq. (18), we obtain, after some rearrangement, for the field envelope in the image plane $z = z_0$ the expression

$$\Psi(x,\tau,z_0) = \frac{\exp\left[\frac{i}{4z_0}(ax^2 + \tau^2/a)\right]}{4\pi i z_0} \int d\xi \int d\zeta\, \Psi_l^-(\xi,\zeta) e^{-\frac{iax\xi}{2z_0}} \times \exp\left(-\frac{i\tau\zeta}{2az_0}\right) \exp\left[-i\xi^2\left(\frac{L_x}{4f} - \frac{a}{4z_0}\right) - i\zeta^2\left(C - \frac{1}{4az_0}\right)\right]. \tag{20}$$

We can infer from Eq. (20) that the quadratic exponential term inside the integral on the right-hand side vanishes provided that

$$L_x = af/z_0, \qquad 4az_0C = 1. \tag{21}$$

It follows from Eq. (21) that the image plane has to be located in the front focal plane of the lens

$$z_0 = f/L_d \implies z_0' = f, \tag{22}$$

and

$$L_t = 4fC. \tag{23}$$

Equation (23) gives a matching condition between the temporal chirp and spatial focal length of the space–time lens to ensure the lens performs a space–time Fourier transform of the field in its focal plane.

Next, we can eliminate the quadratic phase factor in front of the integral in Eq. (20) by adjusting the source position behind the lens. Assuming the conditions [Eqs. (22) and (23)] are met, we can cast Eq. (20) into the form

$$\Psi(x,\tau,f/L_d) \propto \exp\left[\frac{iL_d}{4f}(ax^2 + \tau^2/a)\right] \widetilde{\Psi}_l\left(\frac{axL_d}{2f}, \frac{\tau L_d}{2af}\right). \tag{24}$$

If the source is situated a distance D behind the lens, it follows from Eq. (8) that the Fourier transforms of the fields at the source and on the lens are related as

$$\widetilde{\Psi}_l(K,\Omega) = \widetilde{\Psi}_s(K,\Omega) e^{-iD(a\Omega^2 + K^2/a)}, \tag{25}$$

where the subscript s pertains to the source. On substituting from Eq. (25) into Eq. (24), we can show, after elementary algebra, that the quadratic phase factor in Eq. (24) disappears if the source is placed in the back focal plane of the lens:

$$D = f/L_d \implies D' = f. \tag{26}$$

The matched space–time lens then realizes a scaled Fourier transform of the source in its front focal plane:

$$\Psi_f(x,\tau) \propto \int d\xi \int d\zeta\, \Psi_s(\xi,\zeta) e^{i\left(\frac{L_d}{2f}\right)(ax\xi + \tau\zeta/a)}, \tag{27}$$

where the subscript f refers to the focal plane image.

On substituting from Eq. (17) into Eq. (27) with the source field evaluated at $z = 0$, we derive, after some algebra outlined in Supplement 1, for the PSTV field envelope the expression

$$\Psi_{\mathrm{PSTV}}(x,\tau) \propto e^{il\phi} e^{-r^2/\delta^2} I_l(2r_0 r/\delta^2), \tag{28}$$

where $\delta = 2f/L_d$ is the thickness of the ring and $r_0 = p\delta = 2pf/L_d$ is proportional to the longest (shortest) radius of the vortex ellipse. In the limit $p \gg 1$ ($\delta \ll r_0$), Eq. (28) can be cast into the form (see Supplement 1 for details)

$$\Psi_{\mathrm{PSTV}}(x,\tau) \propto e^{il\phi} e^{-(r-r_0)^2/\delta^2}. \tag{29}$$

Equations (28) and (29) describe the field of a genuine perfect space–time vortex, cf. [17,18]. We illustrate in Fig. S1 in Supplement 1 that the PSTV profile is indeed independent of its OAM content for reasonable values of the topological charge. Such a PSTV has a highly localized peak intensity, and its parameters are easily adjustable by varying the focal length f and chirp C. Notice, however, that for large or small enough a, the shortest ellipse radius can be comparable to its thickness, which distinguishes PSTVs from their circular spatial cousins.

In Fig. 3, we show the intensity, phase, and energy flow of a PSTV with $l = 2$ and variable a, situated in the focal plane of a space–time lens. We can see from the figure that while the aspect ratio of the vortex ring is governed by the magnitude of a, the vortex ring thickness is determined by the angular spectrum parameter p of the Bessel–Gauss source. At the same time, the energy circulates around the dark vortex core, underscoring the genuine vortex structure of the field.

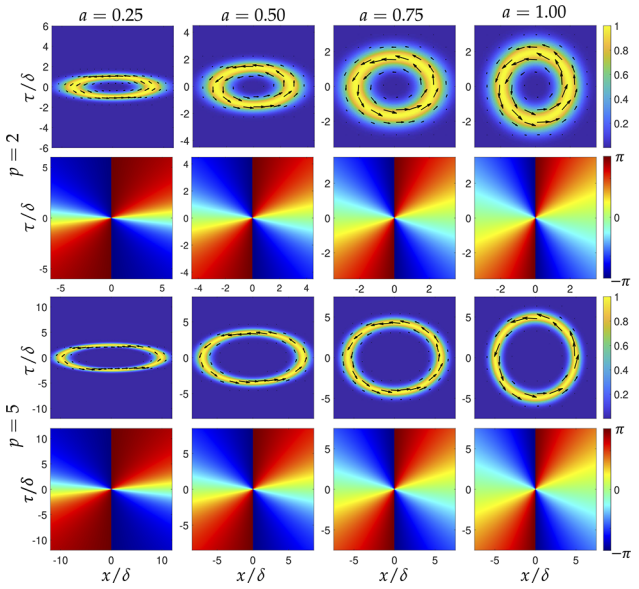

Fig. 3. Intensity (top and third from the top rows) and phase (second from the top and bottom rows) profiles of PSTVs with $l = 2$ and variable p and a in the focal plane of a space–time lens. The energy flow is indicated by the arrows.

In summary, we introduced the concept of a perfect space–time vortex. We have demonstrated that the perfect space–time vortices can be produced by focusing space–time Bessel–Gauss beams with a space–time lens with matching spatial and temporal focal lengths. We expect the discovered space–time vortices to facilitate neutral particle trapping and tweezing along prescribed trajectories in space and time.

Funding. Natural Sciences and Engineering Research Council of Canada (RGPIN-2018-05497).

Acknowledgment. SAP acknowledges support from NSERC (RGPIN-2018-05497) and DH acknowledges an Izaak Walton Killam Postdoctoral Fellowship.

Disclosures. The authors declare no conflicts of interest.

Data availability. Data underlying the results presented in this Letter are not publicly available but may be obtained from the authors upon reasonable request.

Supplemental document. See Supplement 1 for supporting content.

REFERENCES

1. M. Soskin and M. Vasnetsov, in *Progress in Optics*, Vol. 42 (Elseveier, 2001), pp. 219–276.
2. M. R. Dennis, K. O'holleran, and M. J. Padgett, *Progress in Optics*, Vol. 53 (Elsevier, 2009), pp. 293–363.
3. S. A. Ponomarenko, J. Opt. Soc. Am. A **18**, 150 (2001).
4. G. V. Bogatyryova, C. V. Fel'e, P. V. Polyanskii, *et al.*, Opt. Lett. **28**, 878 (2003).
5. L. Allen, M. W. Beijersbergen, R. Spreeuw, *et al.*, Phys. Rev. A **45**, 8185 (1992).
6. A. M. Yao and M. J. Padgett, Adv. Opt. Photonics **3**, 161 (2011).
7. J. Wang, J.-Y. Yang, I. M. Fazal, *et al.*, Nat. Photonics **6**, 488 (2012).
8. K. Gahagan and G. Swartzlander, Opt. Lett. **21**, 827 (1996).
9. J. Chen, C. Wan, and Q. Zhan, Sci. Bull. **63**, 54 (2018).
10. J. H. Lee, G. Foo, E. G. Johnson, *et al.*, Phys. Rev. Lett. **97**, 053901 (2006).
11. X. Li, X. Liu, Q. Wu, *et al.*, APL Photonics **9**, 1 (2024).
12. E. Karimi, G. Zito, B. Piccirillo, *et al.*, Opt. Lett. **32**, 3053 (2007).
13. A. E. Willner and C. Liu, Nanophotonics **10**, 225 (2020).
14. M. Chen, M. Mazilu, Y. Arita, *et al.*, Opt. Lett. **38**, 4919 (2013).
15. A. S. Ostrovsky, C. Rickenstorff-Parrao, and V. Arrizón, Opt. Lett. **38**, 534 (2013).
16. J. García-García, C. Rickenstorff-Parrao, R. Ramos-García, *et al.*, Opt. Lett. **39**, 5305 (2014).
17. P. Vaity and L. Rusch, Opt. Lett. **40**, 597 (2015).
18. J. Pinnell, V. Rodríguez-Fajardo, and A. Forbes, Opt. Lett. **44**, 5614 (2019).
19. C. Wan, A. Chong, and Q. Zhan, eLight **3**, 11 (2023).
20. A. Sukhorukov and V. Yangirova, in *Nonlinear Optics Applications*, Vol. 5949 (SPIE, 2005), pp. 35–43.
21. S. Hancock, S. Zahedpour, A. Goffin, *et al.*, Optica **6**, 1547 (2019).
22. A. Chong, C. Wan, J. Chen, *et al.*, Nat. Photonics **14**, 350 (2020).
23. K. Y. Bliokh and F. Nori, Phys. Rev. A **86**, 033824 (2012).
24. Q. Cao, J. Chen, K. Lu, *et al.*, Sci. Bull. **67**, 133 (2022).
25. S. Hancock, S. Zahedpour, and H. Milchberg, Phys. Rev. Lett. **127**, 193901 (2021).
26. M. Yessenov, L. A. Hall, K. L. Schepler, *et al.*, Adv. Opt. Photonics **14**, 455 (2022).
27. A. Lotti, A. Couairon, D. Faccio, *et al.*, Phys. Rev. A **81**, 023810 (2010).
28. J. Durnin, J. Opt. Soc. Am. A **4**, 651 (1987).
29. J. Durnin, J. Miceli Jr, and J. H. Eberly, Phys. Rev. Lett. **58**, 1499 (1987).
30. B. H. Kolner and M. Nazarathy, Opt. Lett. **14**, 630 (1989).
31. F. J. Marinho and L. M. Bernardo, Opt. Lett. **31**, 1723 (2006).
32. M. Qasymeh, M. Cada, and S. A. Ponomarenko, IEEE J. Quantum Electron. **44**, 740 (2008).
33. J. W. Goodman, in *Introduction to Fourier Optics* (Roberts and Company Publishers, 2005).